POLITECNICO DI TORINO
Repository ISTITUZIONALE

Addressing multi-molecule field-coupled nanocomputing for neural networks with SCERPA

(Article begins on next page)

29 June 2024

Addressing multi-molecule field-coupled nanocomputing for neural networks with SCERPA

Federico Ravera[1] · Giuliana Beretta[1] · Yuri Ardesi[1] · Mariagrazia Graziano[2] · Gianluca Piccinini[1]

Abstract

The molecular field-coupled nanocompunting (molFCN) technology encodes the information in the charge distribution of electrostatically coupled molecules, making it an exciting solution for future beyond-CMOS low-power electronics. Recent literature has shown that multi-molecule molFCN enables the design of devices with tailored unconventional characteristics, such as majority voters working as artificial neurons. This work presents a multi-molecule molFCN neuron model based on the weighted-inputs formulation to estimate molFCN neurons behavior. Then, the introduced model is used to design each neuron of molFCN circuits working as neural networks. In particular, we propose a molFCN neural network operating as an input pattern classifier. The results show the model aptitude in predicting the logic output values for individual neurons and, consequently, entire networks. The model accuracy has been evaluated by comparing the results from the neuron mathematical model with those obtained from the circuit-level simulations conducted with the SCERPA tool. Overall, this study highlights the strategic use of diverse molecules in molFCN layouts, customizing circuit operations, and expanding design possibilities for specific molFCN device functioning.

1 Introduction and background

Molecular Field-Coupled Nanocompunting (molFCN) has been addressed as a promising solution to extend the landscape of Beyond-CMOS technologies. The molFCN implements the Quantum-dot Cellular Automata (QCA) paradigm by encoding logic information in the charge distribution of molecular functional groups, called dots [1, 2]. Figure 1a reports the structure of the bis-ferrocene, one of the most promising molecules studied for molFCN [3]. A pair of electrostatically coupled molecules form the molFCN unit cell, reported in Fig. 1b. Charge within each molecule undergoes motion due to both electrostatic interactions with nearby molecules (E_{sw}) and the influence of an external vertical clock field (E_{ck}), schematically represented in Fig. 1b. A positive E_{ck} pushes charges toward Dot1 and Dot2, facilitating information encoding in the so-called 'Hold' state. In such a case, the charge moves along the cell diagonals to minimize Coulomb's repulsion. The resulting two distinct minimum-energy configurations correspond to the logic states '0' and '1' in Fig. 1c. Conversely, a negative E_{ck} directs charges into Dot3, erasing the encoded information and providing the 'Null' state. The polarization (P_c) is an important figure of merit to evaluate the logic value encoded by a molFCN cell and is computed as in the Eq. (1), where $q1$, $q2$, $q3$, and $q4$ are the dot charges in Fig. 1c [4].

✉ Federico Ravera
federico.ravera@polito.it

Giuliana Beretta
giuliana.beretta@polito.it

Yuri Ardesi
yuri.ardesi@polito.it

Mariagrazia Graziano
mariagrazia.graziano@polito.it

Gianluca Piccinini
gianluca.piccinini@polito.it

1 Department of Electronics and Telecommunications, Politecnico di Torino, Corso Duca degli Abruzzi, 24, 10129 Turin, Italy

2 Department of Applied Science and Technology, Politecnico di Torino, Corso Duca degli Abruzzi, 24, 10129 Turin, Italy
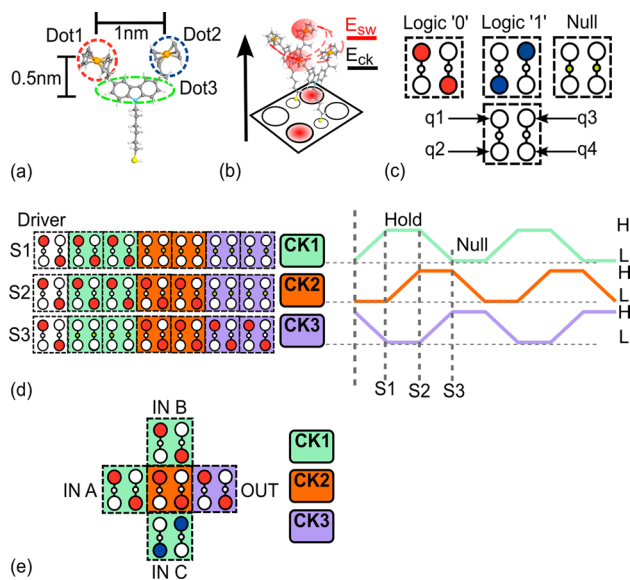
Fig. 1 **a** Bis-ferrocene molecule structure. Dot1, Dot2, and Dot3 are the functional groups where the charge localizes according to surrounding electric fields. **b** Two electrostatically coupled molecules form the molFCN unit cell. E_{sw} and E_{ck} are the two fields influencing the charge position within the molecule. **c** Unit cell schematic and possible charge configurations. **d** Example of a molFCN wire divided into three clock regions. The clock signals CK1, CK2, and CK3 provides the 'Hold' and 'Null' states. **e** Majority Voter gate

$$P_c = \frac{q2 + q3 - q1 - q4}{q1 + q2 + q3 + q4} \tag{1}$$

Information transport occurs through electrostatic interactions within molFCN cells arranged on specific layouts [5, 6]. Figure 1d shows a molFCN wire composed of aligned cells. The information propagation is initiated by the fixed charge distribution of a driver and propagates thanks to the rearrangement of charges within the molecules. The circuit is organized in clock regions, reported in Fig. 1d using different colors, which are activated by different clock signals, namely CK1, CK2, and CK3 in Fig. 1d. The signals alternate between high (H) and low (L) levels, providing the 'Hold' and 'Null' states. The propagation along the wire occurs in three steps, namely S1, S2, and S3. In S1, the first clock region is in 'Hold', and the logic information propagates from the driver into the cells via electrostatic coupling. The logic information then propagates through CK2 in S2 and subsequently into CK3 during S3, finally reaching the circuit output. In general, the clock region successive activation ensures forward propagation and permits information pipelining [7–10]. Moreover, proper cell layout implements digital gates such as the inverter or the Majority Voter (MV), with the latter shown in Fig. 1e [11]. The MV outputs the most frequent input logic, and its layout is divided into three

clock regions to ensure stable computation. The MV central cell activates when IN1, IN2, and IN3 are stable, whereas CK3 ensures stable computed logic value propagation, preventing spurious charge switching [5]. From a circuit-level perspective, this solution eliminates criticalities arising from input propagation delays when longer input branches are considered.

As a whole, molFCN promises theoretically highly reduced power consumption, THz frequencies operations, and room temperature workability [1, 12–15]. Concerning fabrication, molFCN could exploit self-assembly and must rely on sub-nm control of the substrate on which the molecules are deposited and accurate lithography of the clocking structure [11, 16–18].

Aiming to enrich the set of molFCN circuits, we introduced multi-molecule molFCN, demonstrating that using different molecules in a molFCN layout tailors the device functioning [19, 20]. This work extends the analysis by designing molFCN circuits working as multilayered feed-forward neural networks and adapting their functionality to working specifics. First, we introduce the weighted-inputs model used to estimate neuron behavior. Then, we design neural networks formed by four neurons, demonstrating the possibility of customizing the whole circuit functioning by predicting the behavior of the single molFCN neurons in the network. We use the four-neuron network to define the requirements regarding molecule arrangements and clock region activation to obtain correct information propagation. Finally, we use the four-neuron circuit as a building block in designing a molFCN neural network operating as a 3×3 pattern classifier. The outcomes from the single-neuron model are validated by the calculations deriving from the Self-Consistent ElectRostatic Potential Algorithm (SCERPA) tool [11, 21]. The results obtained using SCERPA showcase the possibility of customizing the operation of molFCN circuits by incorporating molecules with distinct electrostatic properties into the layout.

Overall, this study underscores the potential of introducing diverse molecules within a molFCN layout as a strategic solution to customize circuit operations. This approach enhances the design prospects for molFCN circuits, enriching the landscape of available circuits. Additionally, these investigations can guide the synthesis and deposition of molecules to tailor molFCN devices functioning, as already demonstrated for other molecule-based electronics solutions [22–25].
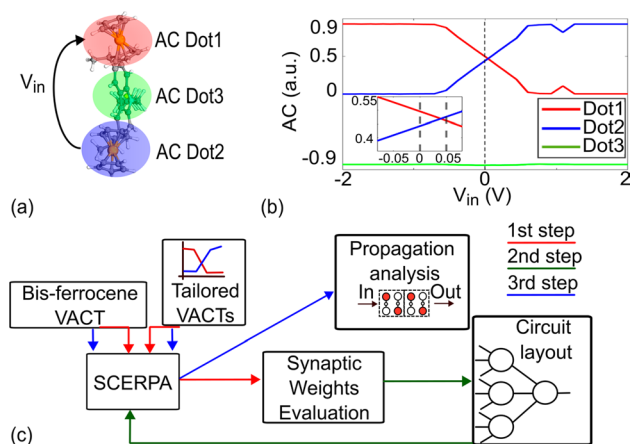
2 Methodology

This work uses the MoSQuiTo (Molecular Simulator Quantum-dot cellular automata Torino) methodology. The methodology analyses molFCN circuits considering the effective

physical behavior, which is fundamental in emerging technologies [5, 11]. The MoSQuiTo approach consists of three steps. First, ab initio simulation analyzes the molecule of interest to evaluate the electronic distribution under the influence of different electric fields. Then, the simulation results are collected to define figures of merit which describe the molecule electronic behavior [11]. This work mainly exploits the Aggregated Charge (AC) and the input voltage V_{in}, both schematized in Fig. 2a. Specifically, the AC is the sum of atomic charges within the molecular dots, whereas V_{in} is determined as the input voltage, evaluated between Dot1 and Dot2, generated by the surrounding electric fields. The relation between these two figures of merit originates the V_{in}-Aggregated Charge Transcharacteristic (VACT), which traces the ACs variation under the influence of different input voltages. The VACT can be evaluated under the effects of different clock fields. In particular, Fig. 2b reports the VACT of the bis-ferrocene molecule obtained by applying a positive E_{ck} [11]. Interestingly, the VACT comprises a region presenting a linear variation of the ACs with the applied V_{in} and a region where the ACs saturate [8]. The minimum voltage to obtain AC saturation is referred to as α [19]. Furthermore, the VACT exhibits asymmetry around $V_{in} = 0$ V, highlighted in the inset in Fig. 2b, indicating a favored charge localization for V_{in} values close to 0 V. This work shows that the asymmetry impacts the isolated neuron and neural network design. In the third step, the extracted characteristics are used by the SCERPA tool to evaluate the

charge distribution in the molecules forming a circuit [11]. Specifically, SCERPA iteratively evaluates the input voltage on each molecule by integrating the electric fields generated by the surrounding molecules ACs and associating it with the charge distribution on the molecular dots using the VACTs.

This work uses SCERPA to design molFCN circuits working as neural networks by inserting molecules with different electrostatic characteristics in the layout, taking advantage of the algorithm flexibility to consider circuits comprising different molecules [21]. Figure 2c schematizes the adopted three-step framework. First, we use the SCERPA tool to evaluate the synaptic weights encoded in the slope of a set of customized VACTs [19], which are associated with ad-hoc defined molecules. In the second step, we employ the just calculated synaptic weights to design artificial neurons and neural networks. Specifically, the synaptic weights are introduced in a model based on the weighted sum of inputs. The model calculates the molFCN neuron polarization, which is associated with the computed logic value [4]. The model assists us in determining the synaptic weights to be positioned at each neuron input to attain predefined circuit functionality, such as input pattern classification. In the third step, SCERPA analyzes the neural circuits comprising bis-ferrocenes and the molecules having tailored VACTs. Precisely, SCERPA evaluates the information propagation considering the different VACTs characterizing the molecules in the circuit [19, 21]. This methodology permits the analysis of the behavior of designed neurons and networks. In addition, we compare the circuit final outputs obtained by SCERPA with those predicted by the mathematical model for each neuron forming the circuit. Our approach, integrating ab initio and ad-hoc molecule characterization, ensures precise circuit functionality and enables in-depth analysis of neuron and network behavior. Overall, this methodology offers a robust foundation for progressing the molFCN circuit landscape.

Fig. 2 **a** Schematic representation of the aggregated charges and the input voltage of a molecule as considered by the MoSQuiTo methodology. **b** V_{in}-to-Aggregated Charge Transcharacteristic (VACT) of the bis-ferrocene molecule subjected to a positive clock field. The zoom-in on the curves around $V_{in} = 0$ V highlights the bis-ferrocene VACT asymmetry. **c** Adopted framework. SCERPA is used in the first step to evaluate the synaptic weights associated with each ad-hoc defined molecule. The synaptic weights are used to evaluate and tailor the neuron working behavior. Finally, SCERPA is again used to evaluate the information propagation through the final circuit, taking the circuit layout and the VACTs as inputs

3 Design and results

This section illustrates the design of molFCN neural networks, delineating the adopted three-step design approach that progresses from individual neurons to multilayered feed-forward networks. First, a single-neuron linear model is introduced. Then, four neurons are connected to form a two-layer neural network. Careful organization of the clock regions and activation processes has been implemented to guarantee accurate information propagation. Finally, the four-neuron circuit layout works as a building block in a molFCN neural network working as a 3x3 input pattern classifier. The classification capabilities underscore the mathematical model aptitude for designing molFCN-based layered

neural networks and the advantages of using multi-molecule solutions to obtain predefined circuit behavior.

## 3.1 Design of a molFCN neuron

In recent years, diverse molecules-based electronics synaptic mechanisms have been explored [19, 26–28]. In particular, authors in [19, 28] proposed two different neuron models compatible with molFCN, each relying on the weighted-inputs formulation [29–31]. Specifically, we proposed in [19] a multi-molecule neuron solution based on the MV layout. Figure 3a shows the neuron layout. This work uses intermolecular distances between molecule centers equal to 0.9 nm and 2 nm along the z and y directions, respectively. The interface cells, namely INT1, INT2, and INT3, and the output cell, labeled saturator cell, are made with molecules with ad-hoc defined VACTs [19]. Bis-ferrocenes compose the central cell, also referred to as the computational cell. V_{INTi}, where $i = 1, 2, 3$, represents the voltages applied at each interface input. The fixed charge arrangement of the driving cells determines these voltages. In particular, the saturator cell is made by molecules having steep transcharacteristics, hereafter labeled as saturator molecules [19]. The saturator molecule used in this work has $\alpha = 0.3$ V. The low α eliminates the risk of output information aberration and provides an entirely digital nature to the neuron [19]. Figure 3b shows the VACTs of the molecules used

to compose the interfaces. The VACTs have α values ranging from +1V to +3V with steps of +0.5V, and the slope of their linear region encodes the synaptic weights [19]. In this work, we use the weight definition reported by equation (2), which links the input voltage applied on each interface to the induced polarization in the computational cell.

$$w_i = \left. \frac{P_c}{V_{INTi}} \right|_{V_{INTi=[-1;1]V}}, \quad \text{with } i = 1, 2, 3 \qquad (2)$$

In Eq. (2) w_1, w_2, and w_3 refer to INT1, INT2, and INT3, respectively. From a circuit-design perspective, the chosen weight formulation considers the interfaces as black boxes with effects on the central cell charge distribution defined by their constituent molecules. Figure 3c shows the details of the weights evaluation. The impact of the defined molecules on each interface is analyzed in SCERPA by varying the corresponding V_{INTi} from -1 to $+1$ V while evaluating P_c, whereas the other interfaces are omitted from the layout to analyze the effect of INTi solely. Figure 3d shows the polarization values obtained through SCERPA by placing the ad-hoc defined molecules on INT3. The weights are calculated based on the slope of the curve linking the SCERPA-evaluated P_c, denoted as P_{cS}, with the input voltages within the range of linear variations of the curves. The inset of Fig. 3d zooms-in on P_{cS} derived from interfaces formed by molecules having α values ranging from 1.5 to 3 V. The curves reveal a minimal influence of those molecules on the computational cell polarization when placed on INT3, providing P_{cS} values ranging from -0.03 to $+0.07$ for $\alpha = 1.5$ V. Noticeably, all the curves are not symmetric to P_{cS} equal to 0, owing to the intrinsic asymmetry of the bis-ferrocene VACT. The same procedure is repeated on each interface molecule, permitting us to separately evaluate the impact of the different ad-hoc defined molecules on the P_c when positioned on INT1, INT2, or INT3. Table 1 reports the evaluated weights. The values indicate that the higher the α, the lower the weight of the corresponding interface, confirming the results obtained in [19]. Thus, the higher the α, the lower the influence on P_c.

The calculated weights are then used to estimate the neuron computation in the design phase. Precisely, we
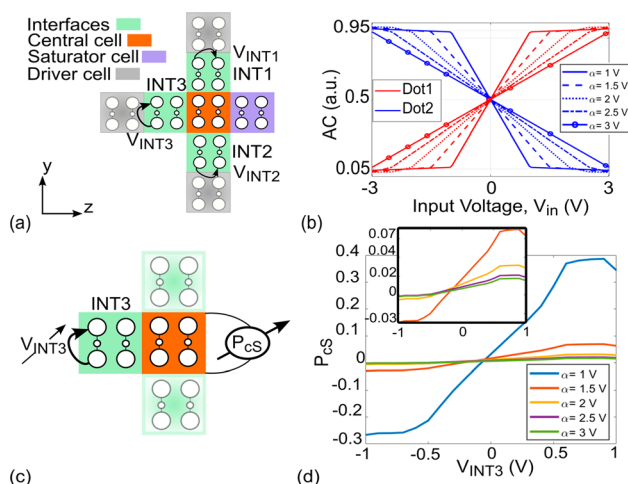
Fig. 3 a Neuron circuit diagram with interfaces receiving distinct input voltages (V_{INTi}, $i = 1, 2, 3$) determined by fixed charge distribution of drivers. The polarization of the central cell P_c depends on the weighted-inputs superposition. A saturator cell made by $\alpha = 0.3$ V molecules is positioned at the circuit output. **b** Ad-hoc defined VACT curves of the interface molecules. **c** Configuration schematic to assess the weight of each ad-hoc molecule for one of three interfaces. The interface of interest undergoes a V_{INTi} sweep from -1 V to $+1$ V while the other two receive $V_{INTi} = 0$ V. **d** P_c curves obtained by applying a V_{INTi} sweep on interface INT3 made by the ad-hoc defined molecules. Inset: zoom-in on the polarization curves for α molecules equal to 1.5 V, 2 V, 2.5 V, and 3 V

Table 1 Weights w_i evaluated by considering the ad-hoc defined molecules on each interface

α (V)	w_1 (V^{-1})	w_2 (V^{-1})	w_3 (V^{-1})
1.0	0.3543	0.3543	0.4560
1.5	0.1523	0.1631	0.0689
2.0	0.1105	0.1169	0.0253
2.5	0.0899	0.0945	0.0153
3.0	0.0774	0.0811	0.0132

evaluate the expected computational cell polarization (P_{cE}) adopting a model relying on the weighted linear combination of the voltages in input to the interfaces as defined by Eq. (3). This approach agrees with the commonly adopted weighted input sum formulation [29–31].

$$P_{cE} = \sum_{i=1}^{3} w_i \cdot V_{INTi} \qquad (3)$$

In this work, the molFCN unit cell configurations '0' and '1' are associated with negative and positive P_{cE}, respectively. To permit the association, we assume the neuron activation function as a step-like function to link the logic behavior to P_{cE} during the design procedure, simplifying the approach compared to the model proposed in [19, 31, 32]. The key distinction lies in the direct link established between P_{cE} and V_{INTi}, differently from the model in [19], which correlates the input voltages to the computational cell and the resulting output voltage of the computational cell itself. Therefore, the novel approach presented in this article favors the design procedure by treating the interfaces as black boxes with known input voltage to induced polarization relationships. This work demonstrates Eq. (3) reliability in predicting the neuron logic response while operating molecules within the linear regions of their transcharacteristics, which guarantees linear weighting during neuron functioning [19].

As an example of neuron computation, consider the following inputs and weights arrangement: $w_1 = 0.3543$ V^{-1}, $V_{INT1} = -0.5$ V ; $w_2 = 0.0945$ V^{-1}, $V_{INT2} = 0.5$ V; $w_3 = 0.0253$ V^{-1}, $V_{INT3} = 0.5$ V. By using Eq. (3), we evaluate $P_{cE} = -0.1179$; thus, a logic '0' is expected as the result of the computation. Figure 4a, b report the SCERPA simulation results. Specifically, the figures present the electrostatic potential 0.2 nm above the Dot1 and Dot2 plane. The bright spots identify positive charges. Figure 4a highlights the computation step of the neuron central cell, which presents P_{cS} equal to -0.2516. The difference between P_{cS} and P_{cE} values derives from the model inherent linearity, which does not consider coupling effects among interfaces and possible molecule nonlinearities. Nevertheless, the model correctly estimates the expected logic value computed on the neuron central cell. Finally, the saturator activation increases P_{cS} to -0.9541, thus leading to the high charge distribution in Fig. 4b and ensuring information stability. Interestingly, Fig. 4b also demonstrates that, for such a set of weights and voltages, the less recurrent logic input drives the neuron output if applied on the most influencing interface. Hence, using different molecules broadens the possibilities associated with the MV gate layout, and the proposed example demonstrates the adopted model efficiency in predicting such situations.
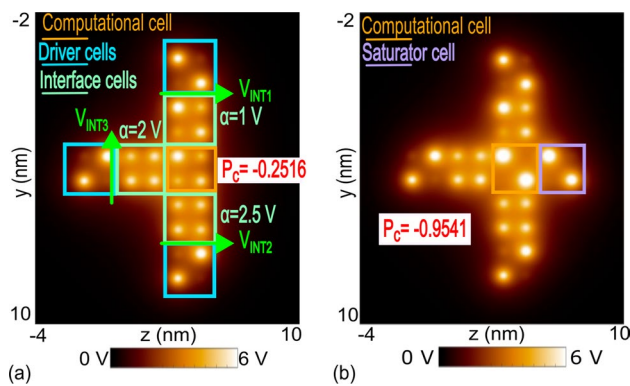
Fig. 4 **a** Neuron computation results provided by SCERPA evaluating the electrostatic potential 0.2 nm above the Dot1 and Dot2 plane. The bright spots highlight the presence of positive charges. The driver cells charge distribution generates the input voltages V_{INTi}, highlighted in light green. The computational cell, in red, shows a charge polarization P_{cS} equal to -0.2516. **b** Activation of the saturator cell, which correctly samples the central cell logic value and enhances its polarization for future propagation
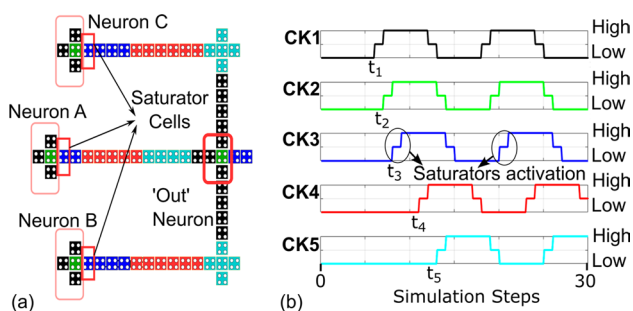

Fig. 5 **a** Layout of a four-neuron neural network and clock region organization for stable information propagation. T-connections are designed considering potential issues arising from molecular electrostatics [5]. **b** The clock signals timing. The colors in the diagram correspond to those in the layout schematic. CK2 and CK3 have been designed to avoid unstable propagation, possibly due to the presence of the highly susceptible saturator molecules and the low P_c in the neuron computational cell

3.2 Simulating a two-layer neural network

This section reports the design of two-layer neural networks using the single neuron presented in Sect. 3.1. The linear model permits to customize the individual functioning of the neurons in the network. Indeed, given that the saturator guarantees a digital facet to each neuron, understanding the isolated neuron behaviors permits us to predict and fine-tune the overall neural network digital functioning. Figure 5a shows the two-layer neural network made of four neurons (NN4). The input layer comprises neurons 'A', 'B', and 'C', whereas the 'Out' neuron works as the output layer. B is-ferrocene molecules make the interconnections among the

neurons. Moreover, Fig. 5a illustrates the five clock regions required to ensure effective information propagation. In particular, T-connections pose a potential challenge in molFCN due to molecular electrostatics, as demonstrated in [5]. Consequently, the layout of these connections needs to be adequately handled. Figure 5b reports the five signals, namely CKi, with i ranging from 1 to 5, governing the clock regions. Each signal consists of High and Low levels separated by a plateau used to model the transitions. The simulation steps in which the first Low-to-High transitions occur are referred to as t_i, $i = [1, 5]$. The three levels correspond to positive, negative, and null E_{ck} values, respectively. The waveforms are designed to ensure correct information propagation. Specifically, proper activation of the saturator molecules is crucial given their high susceptibility to the surrounding fields, primarily due to the low α [33]. Additionally, possible low P_c values indicate unstable charge separation, increasing the risk of information loss. Therefore, as in Fig. 5b, $t2$ and $t3$ are anticipated toward $t1$ compared to $t4$ and $t5$, thus making $t2$–$t1$ and $t3$–$t1$ lower than $t4$–$t3$. Such an insight ensures correct logic value sampling by the saturator molecules, preventing information loss and preserving maximum and stable charge separation conditions [33].

Consider as an example the circuit arrangement reported in Table 2. The P_{cE} for neurons 'A', 'B', and 'C' are +0.2173, +0.1927, and +0.2121, respectively. Thus, three logic '1' are expected. Figure 6 shows the SCERPA results. Figure 6a only focuses on the first computation step, i.e., the propagation of the information in the input layer. Therefore, the charge distribution on the output layer is not relevant. The P_{cS} values evaluated before the saturators activation are +0.0627, +0.2216, and +0.2243 for 'A', 'B', and 'C'. The P_{cS} are close to those predicted by the linear model for neurons 'B' and 'C'. Contrarily, the difference between P_{cE} and P_{cS} for neuron 'A' is relatively high. This condition is probably a result of relevant coupling effects between the interfaces due to the chosen interface configuration. Still, the logic outcomes of the three neurons are correctly predicted. Figure 6b reports the activation of the saturator cells, which drive the polarizations to P_{cS} = +0.8567, P_{cS} = +0.9082 and P_{cS} = +0.9813 for 'A', 'B', and 'C', confirming three logic '1' as outcomes of the first layer of the network. Then, the digital information propagates through the interconnections, reaching the 'Out' neuron interfaces. To estimate P_{cE} for the
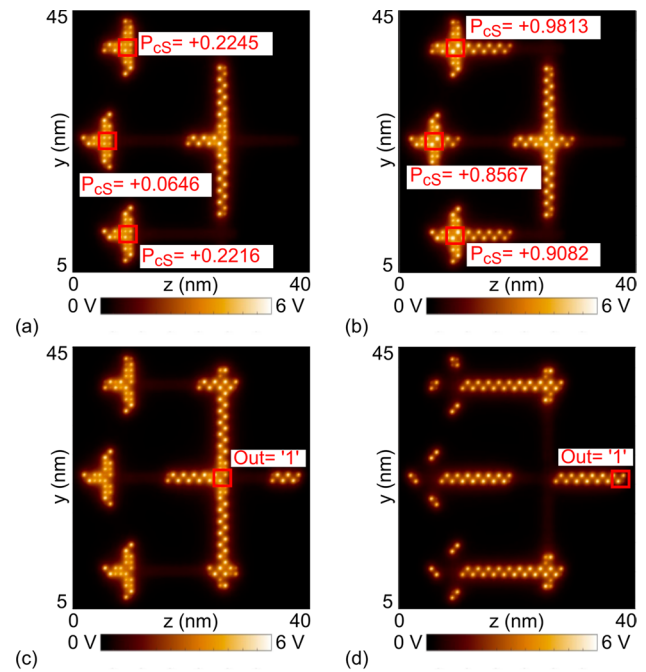
Fig. 6 **a** Input layer neurons computation using the setup reported in Table 2. The P_{cS} values evaluated by SCERPA agree with those obtained using the neuron linear model. **b** The saturator cells activate, maximizing the polarization values of the input layer neurons and initiating the digital propagation. **c** The output layer interfaces weigh the logic values, computing the circuit output. **d** The information propagates correctly along the circuit output wire

output neuron, +0.5 V and −0.5 V are assumed as V_{INTi} for logic '1' and '0', respectively. This assumption reasonably estimates the voltages at the end of bis-ferrocene saturated wires [8]. Indeed, the SCERPA-computed V_{INT1}, V_{INT2}, and V_{INT3} are +0.4254 V, +0.4763 V and +0.4452 V, thus validating the adopted approximation. Considering the chosen output neuron configuration, P_{cE} = +0.5823 derives from Eq. (3), i.e., a logic '1'. Figures 6c, d confirm logic '1' to be the final network output, which is reasonable given that the same logic value is present in input to the three interfaces. Remarkably, Fig. 6c also demonstrates that a new computation is performed in the input layer neurons, proving the chosen clock layout allows pipelining. Overall, the whole circuit outcome is correctly predicted by separately applying the linear model in Eq. (3) on the neurons forming the network.

Table 2 NN4 circuit weights w_i and inputs V_{INTi} for each neuron

Neuron	w_1 (V^{-1})	V_{INT1} (V)	w_2 (V^{-1})	V_{INT2} (V)	w_3 (V^{-1})	V_{INT3} (V)
A	0.3543	0.8	0.1169	−0.5	0.0153	−0.5
B	0.1523	0.8	0.1631	0.5	0.0153	−0.7
C	0.0899	−0.3	0.0945	0.6	0.456	0.4
Out	0.3543		0.3543		0.456	

3.2.1 Case study: error recovery

In the network design phase, the possibility to select neuron interfaces provides a valuable tool for error recovery. Indeed, proper interface selection on the output layer neuron can effectively reduce or nullify the influence of specific interfaces on P_c. Table 3 reports a set of weights and inputs ensuring error recovery. Supposing the desired network output is a logic '0', the selected molecules would provide it. Indeed, the P_{cE} values on the input layer neurons are +0.0521, −0.2154, and −0.0577, i.e., logic '0' for 'B', 'C', and logic '1' for 'A'. Moreover, the interfaces of the output neuron, combined with the ±0.5 V approximation previously discussed, provide a final $P_{cE} = -0.2082$ on the output neuron, leading to a logic '0' as a final result. Opposite to the expectations, Fig. 7a reports neuron 'C' computing a logic '1'. The P_{cS} values evaluated before activating the saturators are +0.0312, −0.3604, and +0.0051 for neurons 'A', 'B', and 'C', respectively. A possible reason for the incorrect prediction is the intrinsic asymmetry to $V_{in} = 0$ V of the bis-ferrocene VACT, leading to wrong logic values when P_c is approximately zero. In general, low polarization values, such as the obtained P_c for neuron 'C', introduce instabilities, possibly leading to unpredictable neuron behavior after the saturator activation. This result showcases how molecule electrostatics significantly influence molFCN circuit design.

(a)

(b)
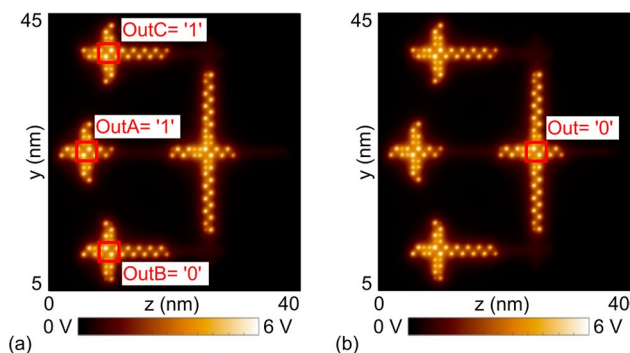
Fig. 7 **a** Computation in the input layer adopting the neurons configurations reported in Table 3. Neuron 'C' computes a logic '1', oppositely to the expectations. **b** The final output computed by the NN4 still aligns with the specifications because of the low w_1. The chosen w_i minimizes the impact of any errors produced by Neuron 'C', demonstrating error recovery possibilities by proper interface selection
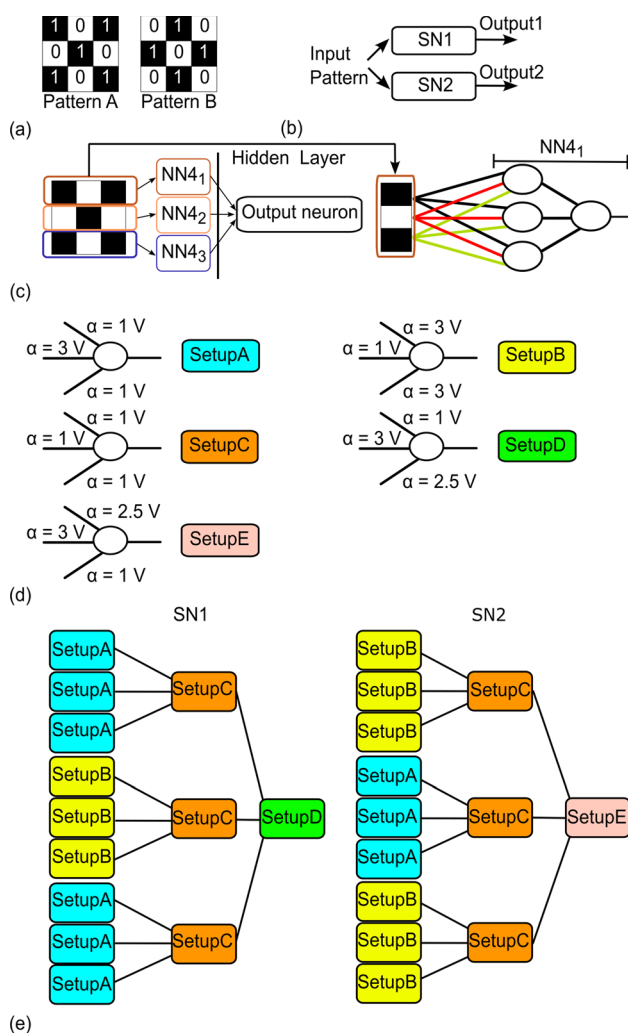
It emphasizes the need for proper molecule characterization to evaluate the circuit behavior in multi-molecule FCN solutions accurately [5, 19, 20].

Besides the incorrect prediction of neuron 'C', the value computed by the output layer is a logic '0', as Fig. 7b reports. Indeed, the chosen interface molecules on INT1 effectively nullify the effects of V_{INT1} on the computational cell polarization. The result demonstrates that the chosen weights effectively suppress the error arising from Neuron 'C', thus increasing the effect of the information coming from neuron 'B'. Therefore, the ability to select neuron interfaces offers a solution for error recovery in molFCN neural networks. Remarkably, the output neuron P_{cE} value considering the computation error becomes −0.1308, which confirms the logic '0' as the output. This example highlights the design flexibility inherent in multi-molecule molFCN circuits and underscores the ability to analyze individual neurons by combining the neuron linear model and the SCERPA calculations. This analysis capability identifies potentially unstable computation conditions and facilitates the strategic arrangement of other neurons within the network to ensure the desired outcomes are consistently achieved.

3.3 Implementation of a molFCN classifier

Finally, we propose the design of a three-layer molFCN neural network working as an input pattern classifier based on the NN4 layout. The network task involves recognizing the 3×3 matrix patterns presented in Fig. 8a according to the following criteria: Pattern A labeled as '10', Pattern B as '01', and '00' or '11' if other patterns are detected. Therefore, a two-bit output parallelism is needed. In Fig. 8a, black squares correspond to input logic '1', while white squares to logic '0'. The circuit is divided into two distinct and autonomous neural networks, denoted as Sub-Networks (SNs). The entire network is schematically illustrated in Fig. 8b. Each SN processes the whole pattern as input, providing one of the two output bits. Figure 8c schematizes each SN detailed internal block scheme. The SNs consist of three NN4 units, labeled as $NN4_1$, $NN4_2$, and $NN4_3$, each receiving input values from a single row of the matrix pattern on its corresponding input layer neurons. Notice that the logic inputs derived from the patterns are provided considering the ±0.5 V approximation introduced previously in this work.

Table 3 Example of neurons w_i and V_{INTi} in the 4NN circuit permitting error recovery

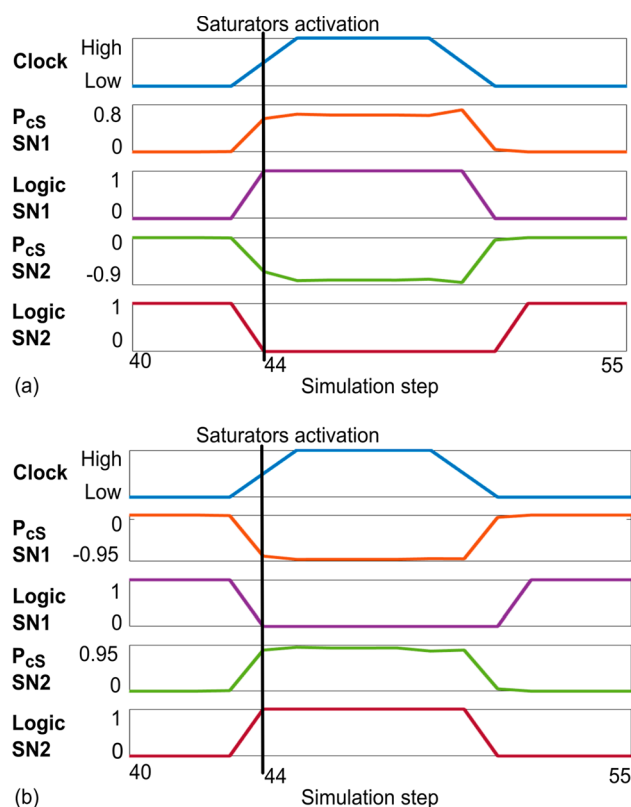| Neuron	w_1 (V^{-1})	V_{INT1} (V)	w_2 (V^{-1})	V_{INT2} (V)	w_3 (V^{-1})	V_{INT3} (V)
A	0.1523	0.5	0.1169	−0.5	0.0689	0.5
B	0.3543	−0.5	0.1631	−0.3	0.0153	0.7
C	0.1105	0.6	0.1169	0.5	0.456	−0.4
Out	0.0774		0.3543		0.0153	

(a)

(b)

(c)

(d)

(e)

Fig. 8 **a** Schematic representation of target input patterns. **b** Complete neural network high-level schematic. **c** Single macro-neuron schematic and inset on the third-row manipulation. **d** Interface configurations of the neurons in the Sub-Networks forming the whole classifier circuit. **e** Sub-Networks neurons setup and connection schematic

(a)

(b)

Fig. 9 Waveforms presenting the polarization and the binary values extracted from SCERPA at the Sub-Networks outputs. **a** Pattern A classification waveforms. The saturator activation leads to maximum charge distributions in the output neurons. The network correctly classifies Pattern A. **b** Pattern B classification waveforms. P_{cS} for the output neurons in SN1 and SN2 follows the expectations providing a final '01'

Furthermore, Fig. 8c depicts the input management of the first row of Pattern A by $NN4_1$. The three bits forming Pattern A upper row are given in inputs to the three neurons of the $NN4_1$ input layer.

Generally, the neurons present in each SN have different interface molecules. Figure 8d reports the chosen setups, whereas Fig. 8e highlights the specific arrangement of the two Sub-Networks. Specifically, a trial-and-error methodology is employed to determine the optimal weights for each neuron interface, aiming to maximize the output accuracy. This selection process evaluates each neuron performance by applying Eq. (3). The maximum classification accuracy is obtained using $\alpha = 1$ V, $\alpha = 2.5$ V, and $\alpha = 3$ V molecules on the input and output layer neurons. In contrast, the neurons

in the hidden layer, i.e., those forming the $NN4_i$ output, have $\alpha = 1$ V molecules on each of the three interfaces, thus behaving as majority voters. Each SN is divided into 19 clock regions governed by the five clock signals presented in Fig. 8b to ensure correct propagation. The proposed molFCN classifier comprises 26 neurons arranged in three layers and 588 molecules, including the interconnections. Besides possibly increasing circuit redundancy, the just-explained circuit design enables the use of the NN4 structure without modifications and streamlines the weight selection process for the different neurons within the circuit.

Figure 9a reports the relevant steps of the information propagation, evaluated with the SCERPA tool, in which the network output layer neurons compute the outputs. Specifically, Fig. 9a reports the P_{cS} and the associated binary values for both SNs with Pattern A as input. The black vertical line indicates the saturator cells activation and the two SNs provide '1' and '0', respectively, classifying Pattern A as expected. The values preceding saturator activation are not considered since depending on random molecular AC states

before the correct information arrives. Analogous considerations can be provided for Pattern B, whose output waveforms behave as expected and are reported in Fig. 9b. Furthermore, we analyzed all the significant pattern variations to evaluate the circuit robustness. As a result, the network correctly classifies Pattern A, Pattern B, or their modifications in 65% of the cases. It is worth noting that variations within the middle row of the binary patterns are particularly critical. Indeed, the middle row is managed by $NN4_2$, whose output is directed toward the interface with the most negligible impact on the computation of the output layer neuron, as determined by the selected configuration. Therefore, possible errors in the middle row can be undetected, leading to the network producing classifications identical to those provided for Pattern A or Pattern B.

Overall, the results related to the molFCN classifier showcase the proposed methodology potential applicability in composing multi-molecule circuits with predetermined behavior. Indeed, the entire network operation can be designed by employing the linear black-box model outlined in this article to characterize each neuron in the layout. For future molFCN neural networks prototyping proper molecule patterning and clocking structures realization must be addressed. In addition, it is necessary to include proper models for power analysis in the framework [10, 11, 34]. Concerning molecule patterning, molFCN can use self-assembly, [16, 35], and proper network functioning could be achieved through single-molecule manipulation techniques, pattern templating [18, 36], and employing crosswiring to achieve complex layouts [20]. Finally, atomic-scale control of the deposition substrate must be considered to achieve the sub-nm patterning precision required by molFCN [16, 37].

4 Conclusion

This work investigates with SCERPA the implementation of molFCN neural networks using multi-molecule circuits. We introduced a model linking input voltages to neuron charge distribution. This model predicted neuron logic output and guided the design and simulation of two-layer networks. The interconnections between neurons were designed with precise clock region organization, preventing information aberration. The results demonstrate the proposed model capabilities to assist the network design to achieve the desired circuit behavior. In particular, we show the case study of an error recovery solution obtained by adequately setting the output neuron interfaces. Finally, we presented a 3×3 pattern classifier comprising 26 neurons and 588 molecules. The classifier effectively discriminates between the two target input patterns, exhibiting an overall accuracy of 65% even in the presence of input pattern variations. The classification accuracy of the proposed network can be further enhanced by refining the proposed single-neuron black-box model. Future research will refine the introduced black-box model to improve classification capabilities and permit comparisons with state-of-the-art solutions. The refinement will include interface coupling contributions and nonlinearities derived from molecules electrostatics in the model.

To sum up, implementing the proposed molFCN neural networks demonstrates the advantages of designing advanced molFCN circuits with specified functioning by adopting multi-molecule solutions. From a more general perspective, the findings and evidence presented in this article can be extrapolated to other technological implementations of QCA circuits. Future works will analyze the proposed molFCN neural network with comprehensive device-level considerations, particularly regarding power dissipation, energy efficiency, and time-sensitivity analysis. Specifically, time-dependent information propagation models and device fabrication-level considerations will be integrated into the MoSQuiTo framework to address comparisons with current state-of-the-art CMOS neural networks.

Declarations

Conflict of interest The authors declare no conflict of interest.

References

1. Lent, C.S., Isaksen, B., Lieberman, M.: Molecular quantum-dot cellular automata. J. Am. Chem. Soc. **125**(4), 1056–1063 (2003)

2. Macrae, R.M.: Mixed-valence realizations of quantum dot cellular automata. J. Phys. Chem. Solids **177**, 111303 (2023)

3. Arima, V., Iurlo, M., Zoli, L., Kumar, S., Piacenza, M., Della Sala, F., Matino, F., Maruccio, G., Rinaldi, R., Paolucci, F., et al.: Toward quantum-dot cellular automata units: thiolated-carbazole linked bisferrocenes. Nanoscale **4**(3), 813–823 (2012)

4. Lu, Y., Lent, C.S.: A metric for characterizing the bistability of molecular quantum-dot cellular automata. Nanotechnology **19**(15), 155703 (2008)

5. Ardesi, Y., Beretta, G., Vacca, M., Piccinini, G., Graziano, M.: Impact of molecular electrostatics on field-coupled nanocomputing and quantum-dot cellular automata circuits. Electronics **11**(2), 276 (2022)

6. Blair, E., Lent, C.: Clock topologies for molecular quantum-dot cellular automata. J. Low Power Electron. Appl. **8**(3), 31 (2018)

7. Lent, C.S., Liu, M., Lu, Y.: Bennett clocking of quantum-dot cellular automata and the limits to binary logic scaling. Nanotechnology **17**(16), 4240 (2006)

8. Ardesi, Y., Pulimeno, A., Graziano, M., Riente, F., Piccinini, G.: Effectiveness of molecules for quantum cellular automata as computing devices. J. Low Power Electron. Appl. **8**(3), 24 (2018)

9. Lent, C.S., Isaksen, B.: Clocked molecular quantum-dot cellular automata. IEEE Trans. Electron. Devices **50**(9), 1890–1896 (2003)

10. Blair, E.P., Yost, E., Lent, C.S.: Power dissipation in clocking wires for clocked molecular quantum-dot cellular automata. J. Comput. Electron. **9**, 49–55 (2010)

11. Ardesi, Y., Garlando, U., Riente, F., Beretta, G., Piccinini, G., Graziano, M.: Taming molecular field-coupling for nanocomputing design. ACM J. Emerging Technol. Comput. Syst. **19**(1), 1–24 (2022)

12. Lent, C.S.: Bypassing the transistor paradigm. Science **288**(5471), 1597–1599 (2000)

13. Wang, Y., Lieberman, M.: Thermodynamic behavior of molecular-scale quantum-dot cellular automata (QCA) wires and logic devices. IEEE Trans. Nanotechnol. **3**(3), 368–376 (2004)

14. Ardesi, Y., Gaeta, A., Beretta, G., Piccinini, G., Graziano, M.: Ab initio molecular dynamics simulations of field-coupled nanocomputing molecules. J. Integrated Circuits Syst. **16**(1), 1–8 (2021)

15. Cui, K., Mali, K.S., Wu, D., Feng, X., Müllen, K., Walter, M., De Feyter, S., Mertens, S.F.: Ambient bistable single dipole switching in a molecular monolayer. Angew. Chem. Int. Ed. **59**(33), 14049–14053 (2020)

16. Graziano, M., Wang, R., Roch, M.R., Ardesi, Y., Riente, F., Piccinini, G.: Characterisation of a bis-ferrocene molecular QCA wire on a non-ideal gold surface. Micro Nano Lett. **14**(1), 22–27 (2019)

17. Verstraete, L., Szabelski, P., Bragança, A.M., Hirsch, B.E., De Feyter, S.: Adaptive self-assembly in 2d nanoconfined spaces: dealing with geometric frustration. Chem. Mater. **31**(17), 6779–6786 (2019)

18. Kocic, N., Blank, D., Abufager, P., Lorente, N., Decurtins, S., Liu, S.-X., Repp, J.: Implementing functionality in molecular self-assembled monolayers. Nano Lett. **19**(5), 2750–2757 (2019)

19. Beretta, G., Ardesi, Y., Graziano, M., Piccinini, G.: Multi-molecule field-coupled nanocomputing for the implementation of a neuron. IEEE Trans. Nanotechnol. **21**, 52–59 (2022)

20. Beretta, G., Ardesi, Y., Piccinini, G., Graziano, M.: Robustness of the in-plane data crossing for molecular field-coupled nanocomputing. In: 2023 IEEE 23rd International Conference on Nanotechnology (NANO). IEEE, pp. 732–736 (2023)

21. Ardesi, Y., Wang, R., Turvani, G., Piccinini, G., Graziano, M.: SCERPA: a self-consistent algorithm for the evaluation of the information propagation in molecular field-coupled nanocomputing. IEEE Trans. Comput. Aided Des. Integr. Circuits Syst. **39**(10), 2749–2760 (2019)

22. Tour, J.M.: Molecular electronics. Synthesis and testing of components. Acc. Chem. Res. **33**(11), 791–804 (2000)

23. Xiang, D., Wang, X., Jia, C., Lee, T., Guo, X.: Molecular-scale electronics: from concept to function. Chem. Rev. **116**(7), 4318–4440 (2016)

24. Bartels, L.: Tailoring molecular layers at metal surfaces. Nat. Chem. **2**(2), 87–95 (2010)

25. Piquero-Zulaica, I., Lobo-Checa, J., Abd El-Fattah, Z.M., Ortega, J.E., Klappenberger, F., Auwärter, W., Barth, J.V.: Engineering quantum states and electronic landscapes through surface molecular nanoarchitectures. Rev. Mod. Phys. **94**(4), 045008 (2022)

26. Hihath, J.: Molecular electronics go synaptic. Nat. Mater. **21**(12), 1346–1347 (2022)

27. Mo, F., Spano, C.E., Ardesi, Y., Piccinini, G., Graziano, M.: Beyond-CMOS artificial neuron: a simulation-based exploration of the molecular-FET. IEEE Trans. Nanotechnol. **20**, 903–911 (2021)

28. Blair, E.P., Koziol, S.: Neuromorphic computation using quantum-dot cellular automata. In: 2017 IEEE International Conference on Rebooting Computing (ICRC), pp. 1–4. IEEE (2017)

29. Krenker, A., Bešter, J., Kos, A.: Introduction to the artificial neural networks. In: Artificial Neural Networks: Methodological Advances and Biomedical Applications. InTech, pp 1–18 (2011)

30. Ojha, V.K., Abraham, A., Snášel, V.: Metaheuristic design of feedforward neural networks: a review of two decades of research. Eng. Appl. Artif. Intell. **60**, 97–116 (2017)

31. Sharma, S., Sharma, S., Athaiya, A.: Activation functions in neural networks. Towards Data Sci. **6**(12), 310–316 (2017)

32. Apicella, A., Donnarumma, F., Isgrò, F., Prevete, R.: A survey on modern trainable activation functions. Neural Netw. **138**, 14–32 (2021)

33. Ardesi, Y., Gnoli, L., Graziano, M., Piccinini, G.: Bistable propagation of monostable molecules in molecular field-coupled nanocomputing. In: 2019 15th Conference on Ph.D. Research in Microelectronics and Electronics (PRIME), pp. 225–228. IEEE (2019)

34. Rahimi, E., Reimers, J.R.: Molecular quantum cellular automata cell design trade-offs: latching vs power dissipation. Phys. Chem. Chem. Phys. **20**(26), 17881–17888 (2018)

35. Vericat, C., Vela, M.E., Corthey, G., Pensa, E., Cortés, E., Fonticelli, M.H., Ibañez, F., Benitez, G., Carro, P., Salvarezza, R.C.: Self-assembled monolayers of thiolates on metals: a review article on sulfur-metal chemistry and surface structures. RSC Adv. **4**(53), 27730–27754 (2014)

36. Escorihuela, E., Concellón, A., Marin, I., Kumar, V.J., Herrer, L., Moggach, S., Vezzoli, A., Nichols, R.J., Low, P.J., Cea, P., et al.: Building large-scale unimolecular scaffolding for electronic devices. Mater. Today Chem. **26**, 101067 (2022)

37. Huang, J.-S., Callegari, V., Geisler, P., Brüning, C., Kern, J., Prangsma, J.C., Wu, X., Feichtner, T., Ziegler, J., Weinmann, P., et al.: Atomically flat single-crystalline gold nanostructures for plasmonic nanocircuitry. Nat. Commun. **1**(1), 150 (2010)